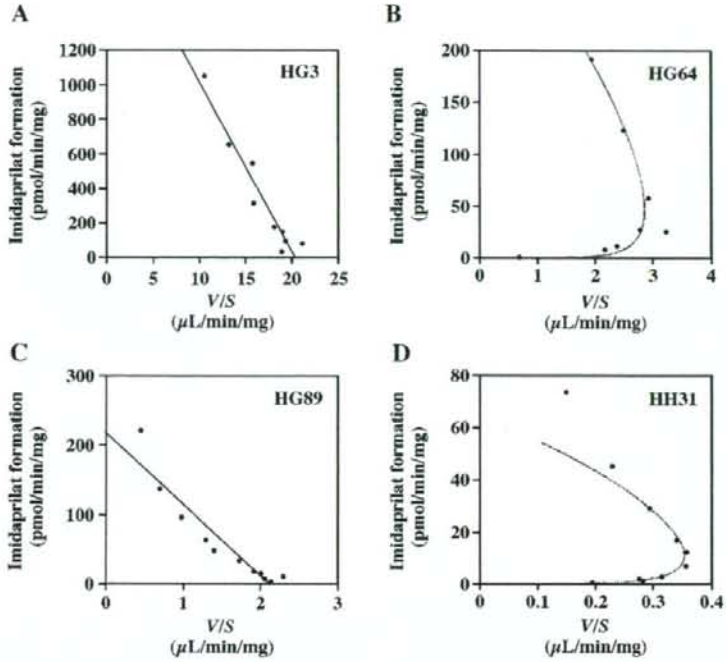

Figure 3. Kinetic analyses of imidaprilat formation catalyzed by individual HLM and HLC. (A) HLM with high activity (HG3); (B) HLM with low activity (HG64); (C) HLC with high activity (HG89); (D) HLC with low activity (HH31). The concentration of imidapril was 2–500 μM. The curved lines (B and D) were estimated by the concentration below 100 μM imidapril. Each point represents the mean of duplicate determinations.

HLM. Eadie-Hofstee plots in RJM and RJC exhibited curved lines at low substrate concentrations ($n = 1.2$). The apparent S_{50} value of RJM was similar to that of RJC, but the CL_{max} value in RJM was higher than that of RJC.

CPGA Formation in Humans and Rats

To clarify the differences of CES1 activity between humans and rats or between liver and jejunum, the CPGA formation was determined at 200 μM

Table 3. Kinetic Parameters of Deraprilat Formation in HLM, HLC, RLM, RLC, RJM, and RJC

	High Affinity Isoform			Low Affinity Isoform			
Enzyme Source	K_m (μM)	V_{max} (nmol/min/mg)	V_{max}/K_m (μL/min/mg)	K_m (μM)	V_{max} (nmol/min/mg)	V_{max}/K_m (μL/min/mg)	n^c
HLM	5.6	1.1	193	460	16.7	36.4	—
HLC	—	—	—	1118[a]	2.8	2.0[b]	1.1
RLM	0.2	0.1	700	33	1.6	49.5	—
RLC	1.7	0.1	29	101	0.8	7.5	—
RJM	—	—	—	28[a]	1.5	32.9[b]	1.2
RJC	—	—	—	41[a]	0.1	1.5[b]	1.2

[a] S_{50}.
[b] CL_{max}.
[c] n, Hill coefficient.

DOI 10.1002/jps

oxybutynin in pooled HLM, pooled HLC, pooled HJM, pooled HJC, RLM, RLC, RJM, and RJC. The pooled HLM showed higher activity (773.5 pmol/min/mg protein) than pooled HLC (38.2 pmol/min/mg protein), pooled HJM (36.8 pmol/min/mg protein), and pooled HJC (5.4 pmol/min/mg protein). No activities were detected in RLM, RLC, RJM, and RJC. Kinetic analyses of the CPGA formation in pooled HLM and HLC were performed and the Eadie-Hofstee plots showed curved lines when the Hill coefficients calculated below 100 μM were 1.5 and 1.1, respectively. As fitted to the Hill equation, the apparent S_{50} values in pooled HLM and HLC were 119.7 and 146.3 μM, respectively and the V_{max} values were 739.1 and 92.4 pmol/min/mg protein, respectively.

Interindividual Variability of CPGA Formation in HLM and HLC

As shown in Figure 2, 15- and 9-fold interindividual variability in the CPGA formation was observed in HLM and HLC, respectively. In HLM, the CPGA formation at 20 μM oxybutynin showed the highest in HG3 (375.3 pmol/min/mg protein) and the lowest in HH47 (25.1 pmol/min/mg protein). In HLC, the CPGA formation showed the highest in HG3 (72.8 pmol/min/mg protein) and the lowest in HG64 (7.6 pmol/min/mg protein) (Fig. 4). The CPGA formation was significantly correlated between individual HLM and HLC from the same donors ($n = 6$, $r = 0.89$, $p < 0.05$). Moreover, the CPGA formation was significantly correlated with the imidaprilat formation in both HLM ($r = 0.98, p < 0.001$) and HLC ($r = 0.97$, $p < 0.001$).

Kinetic Analysis of CPGA Formation in Individual HLM and HLC

Kinetic analyses of CPGA formation were performed in individual HLM and HLC (Tab. 4). The apparent K_m values of CPGA formation in HLM and HLC were similar. CPGA formation in HLM and HLC with high activities also exhibited curved lines in the Eadie-Hofstee plots (Fig. 5) and their Hill coefficients calculated below 100 μM showed 1.2 and 1.6, respectively. The Eadie-Hofstee plots in HLM with low activities were monophasic but those in HLC were curved.

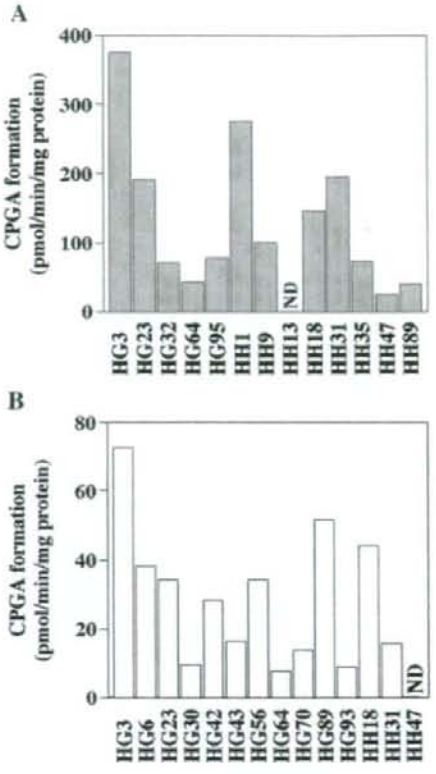

Figure 4. Interindividual variability of CPGA formation in 13 HLM (A) and in 13 HLC (B). The concentration of oxybutynin was 20 μM. Each column represents the mean of duplicate determinations. ND, not detected.

DISCUSSION

It is important to clarify the characteristics of drug metabolizing enzymes for understanding the *in vivo* pharmacokinetics. CES1 is involved in the metabolism of various prodrugs such as imidapril and capecitabine. To investigate the formation of an active metabolite from the prodrug would be important for drug development. However, sufficient information on the enzymatic properties of CES1 is not available. In the preliminary study, the imidaprilat and CPGA formation in HLM and HLC were inhibited by BNPP, but not by loperamide which was a potent CES2 inhibitor,[21] indicating that CES1 would be involved in these hydrolysis. In the present study, kinetic analyses of drugs hydrolyzed by CES1 were performed in humans and rats.

Table 4. Kinetic Parameters of CPGA Formation in Individual HLM and HLC

Enzyme Source	Activity	Donor	K_m (μM)	V_{max} (pmol/min/mg)	V_{max}/K_m (μL/min/mg)	n	Model
HLM	High	HG3	75[a]	1187	10.0[b]	1.2 (1.2[c])	Hill
	Low	HH47	123	107	0.9	—	Michaelis-Menten
HLC	High	HH18	93[a]	283	2.9[b]	1.0 (1.6[c])	Hill
	Low	HG64	94[a]	38	0.3[b]	1.1 (1.5[c])	Hill

n, Hill coefficient calculated using all concentrations of oxybutynin.
[a]S_{50}.
[b]CL_{max}.
[c]Hill coefficient calculated below 100 μM oxybutynin.

In this study, it was first clarified that imidaprilat and CPGA formation showed sigmoidal kinetics in pooled HLM and HLC. The Eadie-Hofstee plots in pooled HLM and HLC were curved sharply at low substrate concentrations (less than 20 μM). The Hill coefficients were estimated to be close to 1.0 when we used all points ranging from 2 to 500 μM imidapril and from 5 to 500 μM oxybutynin. However, the Hill coefficients appeared higher when plotting the activities at only low substrate concentrations. For example, in the CPGA formation in pooled HLM, the Hill coefficient was 1.5 at from 5 to 100 μM oxybutynin. CES1 may behave differently at high substrate concentrations compared with low concentrations. Based on the Eadie-Hofstee plots, it is suggested that CES1 would function allosterically.

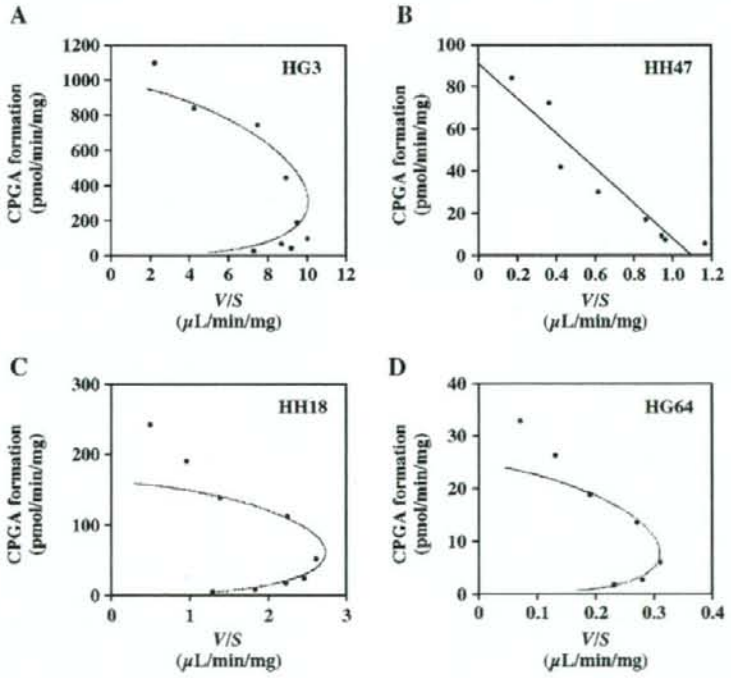

Figure 5. Kinetic analyses of CPGA formation catalyzed by individual HLM and HLC. (A) HLM with high activity (HG3); (B) HLM with low activity (HH47); (C) HLC with high activity (HH18); (D) HLC with low activity (HG64). The concentration of oxybutynin was 4–500 μM. The curved lines (A, C, and D) were estimated by the concentration below 100 μM oxybutynin. Each point represents the mean of duplicate determinations.

Imidaprilat formation in RLM and RLC exhibited Michaelis-Menten kinetics, suggesting that species difference exists. In rat CESs, many isoforms have been identified.[22] In the preliminary study, a specific CES inhibitor, BNPP, inhibited the imidaprilat formation in all enzyme sources from rats. Yamada et al.[23] reported that imidapril was hydrolyzed more efficiently by CES in rat liver than in other tissues. Thus, rat CES should be involved in imidapril metabolism. In the case of another angiotensin-converting enzyme inhibitor, derapril, the kinetics of deraprilat formation in all enzyme sources were different from those of imidaprilat formation. However, derapril has a similar chemical structure to imidapril. Derapril is more bulky than imidapril, thus such a difference might be responsible for the difference in kinetics. On the other hand, no CPGA formation in rats could be detected, suggesting that large species difference would also exist.

In both humans and rats, the V_{max}/K_m or CL_{max} values of the imidaprilat formation in liver were higher than those in jejunum. Human CES1 is mainly expressed in the liver but is found at low expression levels in the small intestine.[24] The differences in the enzymatic activities between liver and jejunum may be explained by the expression levels of CES1. In comparison with microsomes and cytosol in the present study, the V_{max}/K_m or CL_{max} values of imidaprilat formation in all microsomes were higher than those in cytosol. Our previous report indicated that the hydrolysis activity of cytosolic CES1 might be almost equal to that of microsomal CES when taking the protein concentrations into account.[3] Cytosolic proteins are approximately five-fold higher than microsomal proteins in human liver S9.[25] The contribution of cytosolic CES to hydrolysis may be as important as that of microsomal CES in both humans and rats. Recently, human CES1A1 (AB119997) and CES1A2 (AB119998) were registered in GenBank. Their coding regions showed high homology and they had four amino acid differences in their N-terminal regions.[26] Hosokawa et al.[27] speculated that CES1 genes had inverted duplication and were differently regulated at the transcriptional level. However, there are few reports on the differences in the structure, enzymatic activity, and substrate specificity between CES1A1 and CES1A2.

In the present study, there was large interindividual variability in the CES1 activities, which was consistent with previous reports.[3,28] In the imidaprilat formation, the Eadie-Hofstee plot in HLM with low activity was curved sharply around 20 μM, indicating that CES1 may show autoactivation kinetics. The kinetics of imidaprilat formation appeared different depending on the individuals. HLM and HLC with low activity exhibited sigmoidal kinetics in the imidaprilat formation. Since the serum concentration (79 nM) of imidapril in clinical doses (10 mg/day) is lower than the S_{50} value, sigmoidal kinetics may result in the low serum concentration in individuals in comparison with the Michaelis-Menten kinetics. The allosteric effects of CES1 could affect the interindividual variability, but further studies are needed to clarify this issue. There was large interindividual variability in the CPGA formation as in the imidaprilat formation. In individual HLM and HLC, the CPGA formation was significantly correlated with the imidaprilat formation (HLM, $r = 0.98$, $p < 0.001$; HLC, $r = 0.97$, $p < 0.001$), which has been reported to be specifically catalyzed by CES1.[6] Takai et al.[6] also demonstrated that oxybutynin was hydrolyzed by carboxylesterase with pI 4.5, which seems to be CES2, but loperamide did not inhibit the CPGA formation in pooled HLM and HLC in this study. Recombinant CESs are needed to identify the catalytic isoforms, but are not now available. In the present experimental condition, the CPGA formation would be catalyzed by human CES1 because of the significant correlation between the imidaprilat and CPGA formation. In individual HLM and HLC with high activities, the kinetics of the CPGA formation exhibited sigmoidal curves. However, imidaprilat formation in high activity individuals showed Michaelis-Menten kinetics, suggesting that CES1 may behave differently depending on the substrates.

Recently, crystal structures of human CES1 have been reported in complexes with several substrates.[29,30] In such reports, human CES1 contains three ligand binding sites, an active site, a side door, and a Z-site.[31] Bencharit et al.[32] reported that some compounds could bind to the Z-site and that the Z-site may function as an allosteric site, which may be related to the sigmoidal kinetics observed in the present study. Cytochrome P450 3A4 (CYP3A4) has a surface ligand binding site near its active site that may play a role in the recognition of substrates and in the allosteric behavior.[33] The surface ligand binding site of CYP3A4 may correspond to the Z-site of CES1.

Genetic polymorphisms of various drug metabolizing enzymes have been reported and many mutants can affect the catalytic activity.[34] In the case of CYP2B6, the G516T substitution in exon 4 altered the Michaelis-Menten kinetics to sigmoidal kinetics for 7-ethoxycoumarin *O*-deethylase activity.[35] Some single nucleotide polymorphisms (SNPs) can change the kinetic behavior. In the CES1 gene, several SNPs have been identified.[36] Geshi et al.[37] reported that a A(-816)C SNP on the CES1A2 promoter region might affect its transcriptional activity and the elevated responsiveness to imidapril. It is surmised that the genetic polymorphism of CES1 might be responsible for the allosteric effect, but further study is needed to clarify this issue.

In conclusion, species and tissue differences in the CES1 kinetics were elucidated. Moreover, we first clarified that CES1 exhibited sigmoidal kinetics depending on the substrates and the donors of the enzymes. Information on species and tissue differences in CES1 kinetics is important for drug development. For understanding the pharmacokinetics of a CES substrate, we should accumulate basic information concerning the enzyme characteristics. Because the allosteric effects of CES1 may be one of the determinants of the large interindividual variability in clinical doses, the allosteric mechanism should be clarified.

ACKNOWLEDGMENTS

We acknowledge Tanabe Seiyaku for kindly providing imidapril and imidaprilat and Takeda Pharmaceutical for kindly supplying derapril. We thank Mr. Brent Bell for reviewing the manuscript.

REFERENCES

1. Satoh T, Hosokawa M. 2006. Structure, function and regulation of carboxylesterases. Chem Biol Interact 162:195–211.
2. Inoue M, Morikawa M, Tsuboi M, Sugiura M. 1979. Species difference and characterization of intestinal esterase on the hydrolizing activity of ester-type drugs. Jpn J Pharmacol 29:9–16.
3. Tabata T, Katoh M, Tokudome S, Hosokawa M, Chiba K, Nakajima M, Yokoi T. 2004. Bioactivation of capecitabine in human liver: Involvement of the cytosolic enzyme on 5′-deoxy-5-fluorocytidine formation. Drug Metab Dispos 32:762–767.
4. Schaid DJ, McDonnell SK, Wang L, Cunningham JM, Thibodeau SN. 2002. Caution on pedigree haplotype inference with software that assumes linkage equilibrium. Am J Hum Genet 71:992–995.
5. Satoh T, Taylor P, Bosron WF, Sanghani SP, Hosokawa M, LaDu BN. 2002. Current progress on esterases: From molecular structure to function. Drug Metab Dispos 30:488–493.
6. Takai S, Matsuda A, Usami Y, Adachi T, Sugiyama T, Katagiri Y, Tatematsu M, Hirano K. 1997. Hydrolytic profile for ester- or amide-linkage by carboxylesterases pI 5.3 and 4.5 from human liver. Biol Pharm Bull 20:869–873.
7. Sun Z, Murry DJ, Sanghani SP, Davis WI, Kedishvili NY, Zou Q, Hurley TD, Bosron WF. 2004. Methylphenidate is stereoselectively hydrolyzed by human carboxylesterase CES1A1. J Pharmacol Exp Ther 310:469–476.
8. Shi D, Yang J, Yang D, LeCluyse EL, Black C, You L, Akhlaghi F, Yan B. 2006. Anti-influenza prodrug oseltamivir is activated by carboxylesterase human carboxylesterase 1, and the activation is inhibited by antiplatelet agent clopidogrel. J Pharmacol Exp Ther 319:1477–1484.
9. Yamaori S, Fujiyama N, Kushihara M, Funahashi T, Kimura T, Yamamoto I, Sone T, Isobe M, Ohshima T, Matsumura K, Oda M, Watanabe K. 2006. Involvement of human blood arylesterases and liver microsomal carboxylesterases in nafamostat hydrolysis. Drug Metab Pharmacokinet 21: 147–155.
10. Razzetti R, Acerbi D. 1995. Pharmacokinetic and pharmacologic properties of delapril, a lipophilic nonsulfhydryl angiotensin-converting enzyme inhibitor. Am J Cardiol 75:7F–12F.
11. Shinozaki Y, Monden R, Manaka A, Hisa H, Naito S, Igarashi T, Sakai H, Iwata Y, Kasama T. 1986. Studies on metabolic fate of oxybutynin hydrochloride (3) metabolism in human and dog and the site of biotransformation and the effect on enzymes induction in the rats. Xenobio Metabol Dispos 1: 13–24.
12. Satoh T, Hosokawa M. 1998. The mammalian carboxylesterases: From molecules to functions. Annu Rev Pharmacol Toxicol 38:257–288.
13. Li B, Sedlacek M, Manoharan I, Boopathy R, Duysen EG, Masson P, Lockridge O. 2005. Butyrylcholinesterase, paraoxonase, and albumin esterase, but not carboxylesterase, are present in human plasma. Biochem Pharmacol 70:1673–1684.
14. Godin SJ, Scollon EJ, Hughes MF, Potter PM, DeVito MJ, Ross MK. 2006. Species differences in the in vitro metabolism of deltamethrin and esfenvalerate: Differential oxidative and hydrolytic metabolism by humans and rats. Drug Metab Dispos 34:1764–1771.
15. Crow JA, Borazjani A, Potter PM, Ross MK. 2007. Hydrolysis of pyrethroids by human and rat tissues:

Examination of intestinal, liver and serum carboxylesterases. Toxicol Appl Pharmacol 221:1–12.
16. Emoto C, Yamazaki H, Iketaki H, Yamasaki S, Satoh T, Shimizu R, Suzuki S, Shimada N, Nakajima M, Yokoi T. 2001. Cooperativity of alpha-naphthoflavone in cytochrome P450 3A-dependent drug oxidation activities in hepatic and intestinal microsomes from mouse and human. Xenobiotica 31:265–275.
17. Mabuchi M, Kano Y, Fukuyama T, Kondo T. 1999. Determination of imidapril and imidaprilat in human plasma by high-performance liquid chromatography-electrospray ionization tandem mass spectrometry. J Chromatogr B Biomed Sci Appl 734:145–153.
18. Ito H, Yasumatsu M, Usui Y. 1985. Determination of a new angiotensin converting enzyme inhibitor (CV-3317) and its metabolites in serum and urine by high-performance liquid chromatography. Fukuoka Igaku Zasshi 76:441–450.
19. Malcolm K, Woolfson D, Russell J, Tallon P, McAuley L, Craig D. 2003. Influence of silicone elastomer solubility and diffusivity on the in vitro release of drugs from intravaginal rings. J Control Release 90: 217–225.
20. Houston JB, Kenworthy KE. 2000. In vitro-in vivo scaling of CYP kinetic data not consistent with the classical Michaelis-Menten model. Drug Metab Dispos 28:246–254.
21. Quinney SK, Sanghani SP, Davis WI, Hurley TD, Sun Z, Murry DJ, Bosron WF. 2005. Hydrolysis of capecitabine to 5′-deoxy-5-fluorocytidine by human carboxylesterases and inhibition by loperamide. J Pharmacol Exp Ther 313:1011–1016.
22. Mentlein R, Ronai A, Robbi M, Heymann E, von Deimling O. 1987. Genetic identification of rat liver carboxylesterases isolated in different laboratories. Biochim Biophys Acta 913:27–38.
23. Yamada Y, Otsuka M, Takaiti O. 1992. Metabolic fate of the new angiotensin-converting enzyme inhibitor imidapril in animals. 7th communication: In vitro metabolism. Arzneimittelforschung 42: 507–512.
24. Xu G, Zhang W, Ma MK, McLeod HL. 2002. Human carboxylesterase 2 is commonly expressed in tumor tissue and is correlated with activation of irinotecan. Clin Cancer Res 8:2605–2611.
25. Komatsu T, Yamazaki H, Shimada N, Nagayama S, Kawaguchi Y, Nakajima M, Yokoi T. 2001. Involvement of microsomal cytochrome P450 and cytosolic thymidine phosphorylase in 5-fluorouracil formation from tegafur in human liver. Clin Cancer Res 7:675–681.
26. Tanimoto K, Kaneyasu M, Shimokuni T, Hiyama K, Nishiyama M. 2007. Human carboxylesterase 1A2 expressed from carboxylesterase 1A1 and 1A2 genes is a potent predictor of CPT-11 cytotoxicity in vitro. Pharmacogenet Genomics 17:1–10.
27. Hosokawa M, Furihata T, Yaginuma Y, Yamamoto N, Koyano N, Fujii A, Nagahara Y, Satoh T, Chiba K. 2007. Genomic structure and transcriptional regulation of the rat, mouse, and human carboxylesterase genes. Drug Metab Rev 39:1–15.
28. Tang M, Mukundan M, Yang J, Charpentier N, LeCluyse EL, Black C, Yang D, Shi D, Yan B. 2006. Antiplatelet agents aspirin and clopidogrel are hydrolyzed by distinct carboxylesterases, and clopidogrel is transesterificated in the presence of ethyl alcohol. J Pharmacol Exp Ther 319:1467–1476.
29. Bencharit S, Morton CL, Hyatt JL, Kuhn P, Danks MK, Potter PM, Redinbo MR. 2003. Crystal structure of human carboxylesterase 1 complexed with the Alzheimer's drug tacrine: From binding promiscuity to selective inhibition. Chem Biol 10: 341–349.
30. Fleming CD, Bencharit S, Edwards CC, Hyatt JL, Tsurkan L, Bai F, Fraga C, Morton CL, Howard-Williams EL, Potter PM, Redinbo MR. 2005. Structural insights into drug processing by human carboxylesterase 1: Tamoxifen, mevastatin, and inhibition by benzil. J Mol Biol 352:165–177.
31. Bencharit S, Morton CL, Xue Y, Potter PM, Redinbo MR. 2003. Structural basis of heroin and cocaine metabolism by a promiscuous human drug-processing enzyme. Nat Struct Biol 10:349–356.
32. Bencharit S, Edwards CC, Morton CL, Howard-Williams EL, Kuhn P, Potter PM, Redinbo MR. 2006. Multisite promiscuity in the processing of endogenous substrates by human carboxylesterase 1. J Mol Biol 363:201–214.
33. Williams PA, Cosme J, Vinkovic DM, Ward A, Angove HC, Day PJ, Vonrhein C, Tickle IJ, Jhoti H. 2004. Crystal structures of human cytochrome P450 3A4 bound to metyrapone and progesterone. Science 305:683–686.
34. Bosch TM, Meijerman I, Beijnen JH, Schellens JH. 2006. Genetic polymorphisms of drug-metabolising enzymes and drug transporters in the chemotherapeutic treatment of cancer. Clin Pharmacokinet 45:253–285.
35. Ariyoshi N, Miyazaki M, Toide K, Sawamura YI, Kamataki T. 2001. A single nucleotide polymorphism of CYP2B6 found in Japanese enhances catalytic activity by autoactivation. Biochem Biophys Res Commun 281:1256–1260.
36. Marsh S, Xiao M, Yu J, Ahluwalia R, Minton M, Freimuth RR, Kwok PY, McLeod HL. 2004. Pharmacogenomic assessment of carboxylesterases 1 and 2. Genomics 84:661–668.
37. Geshi E, Kimura T, Yoshimura M, Suzuki H, Koba S, Sakai T, Saito T, Koga A, Muramatsu M, Katagiri T. 2005. A single nucleotide polymorphism in the carboxylesterase gene is associated with the responsiveness to imidapril medication and the promoter activity. Hypertens Res 28:719–725.

Human Cytochrome P450 2A13 Efficiently Metabolizes Chemicals in Air Pollutants: Naphthalene, Styrene, and Toluene

Tatsuki Fukami, Miki Katoh, Hiroshi Yamazaki,† Tsuyoshi Yokoi, and Miki Nakajima*

Drug Metabolism and Toxicology, Division of Pharmaceutical Sciences, Graduate School of Medical Science, Kanazawa University, Kakuma-machi, Kanazawa 920-1192, Japan

Human P450 2A13 is the most efficient enzyme for catalyzing the metabolism of nicotine and metabolic activation of 4-(methylnitrosamino)-1-(3-pyridyl)-1-butanone (NNK). It is conceivable that P450 2A13 also metabolizes chemicals in air pollutants because this enzyme is highly expressed in the respiratory tract. In this study, we investigated the possibility that P450 2A13 can metabolize naphthalene, styrene, and toluene, which are included in air pollutants as well as tobacco smoke, although they were known to be metabolized by P450 1A2 or 2E1. We found that P450 2A13 catalyzed 1- and 2-naphthol formations from naphthalene with higher intrinsic clearances (*k*cat/*K*m) (3.1- and 2.2-fold, respectively) than P450 1A2 and also more efficiently catalyzed the styrene 7,8-oxide formation from styrene and the benzylalcohol formation from toluene than P450 2E1. The overlapping substrate specificity of P450 2A13 with P450 2E1 was supported by the finding that P450 2A13 catalyzed chlorzoxazone 6-hydroxylation (8-fold higher value of *k*cat/*K*m) and *p*-nitrophenol 2-hydroxylation (19-fold higher value of *k*cat/*K*m), which are marker activities of P450 2E1. Thus, we found that P450 2A13 metabolizes diverse environmental chemicals and has overlapping substrate specificities of P450 1A2 and 2E1, suggesting that P450 2A13 plays important roles in the local metabolism of environmental chemicals in the respiratory tract related to toxicity or carcinogenicity.

Introduction

The human cytochrome P450 (P450[1]) 2A subfamily comprises three genes: *P450 2A6*, *2A7*, and *2A13* (*1*). Among them, *P450 2A6* and *2A13* encode functional enzymes (*2, 3*). P450 2A13 is the most efficient enzyme in the metabolism of nicotine and metabolic activation of 4-(methylnitrosamino)-1-(3-pyridyl)-1-butanone (NNK) with a substrate specificity similar to that of P450 2A6 (*3, 4*) because of the high amino acid identity between them (93.5%) (*1*). P450 2A6 is predominantly expressed in the liver, whereas P450 2A13 is predominantly expressed in the respiratory tract, with the highest level in the nasal mucosa, followed by the lung and trachea (*3, 5, 6*). P450 2A13 also metabolizes aflatoxin B_1 (*7*). Recently, we found that P450 2A13 can metabolize phenacetin, theophylline (*8*), and 4-aminobiphenyl (*9*), although P450 2A6 showed no or negligible activity. Thus, the substrate specificity of P450 2A13 does not necessarily overlap with that of P450 2A6. Since P450 2A13 is mainly expressed in the respiratory tract, it is feasible that P450 2A13 may catalyze the metabolism of environmental chemicals in air pollutants.

In cigarette smoke, more than 4,000 identified constituents are present. Among them, more than 200 constituents are known to be carcinogens or toxicants. Inhaled cigarette smoke deposits chemicals in the bronchial airway passages and lung. Many carcinogens require activation by enzymes such as P450 to elicit the carcinogenicity or toxicity. Naphthalene is a bicyclic aromatic compound included in cigarette smoke and diesel fumes (*10*). It is also used in the manufacturing of naphthylamines, anthranilic and phthalic acids, and synthetic resins

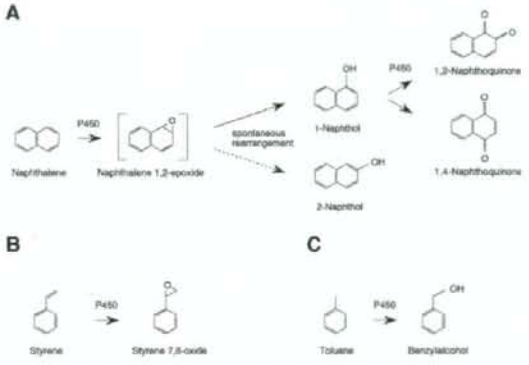

Figure 1. Metabolic pathways of (A) naphthalene, (B) styrene, and (C) toluene by human P450.

(*11, 12*). Naphthalene is mainly converted to 1-naphthol and further to 1,2-naphthoquinone and 1,4-naphthoquinone, the ultimate toxic compounds (Figure 1A). An in vitro study revealed that these naphthoquinones have similar cytotoxicity (*13*). Recently, it has been reported that multiple P450 isoforms are involved in the metabolism of naphthalene and 1-naphthol and that P450 1A2 has the highest activity (*14*). Since the target organs of the toxicity of naphthalene are the lung and bronchus (*15, 16*), and since P450 1A2 is expressed only in the liver, the naphthalene metabolism by the P450 expressed in the respiratory tract should be characterized. Styrene and toluene are widely used as industrial solvents (*17, 18*). High occupational exposure to them results in significant toxicity in the nervous system as well as many organs (*19, 20*). Since they are present in many household products such as aerosols, degreasers, glues, and paints, the general population is likely to be exposed to them. It has been demonstrated that most of the adverse effects of styrene can be attributed to a metabolite, styrene 7,8-oxide (*19*).

* To whom correspondence should be addressed. Tel/Fax: +81-76-234-4407. E-mail: nmiki@kenroku.kanazawa-u.ac.jp.

† Current address: Laboratory of Drug Metabolism and Pharmacokinetics, Shawa Pharmaceutical University, Machida, Tokyo 194-8543, Japan.

[1] Abbreviations: NNK, 4-(methylnitrosamino)-1-(3-pyridyl)-1-butanone; NPR, NADPH-P450 reductase; P450, cytochrome P450.

10.1021/tx700325f CCC: $40.75
Published on Web 02/12/2008

The epoxidation of styrene is known to be catalyzed by P450 2E1 and 2B6 to a similar extent (Figure 1B) (*21*). The toxicity of toluene is assumed to depend on the duration and magnitude of exposure as well as its metabolic fate. In vitro studies suggested that methyl-hydroxylation by P450 2E1 is a primary detoxification pathway (Figure 1C) (*22, 23*).

In general, the liver is the principal tissue of the metabolism of xenobiotics, but the lung or bronchus that is directly exposed to tobacco carcinogens or air pollutants would also play an important role in the metabolism of xenobiotics. In this study, we investigated whether P450 2A13 has catalytic ability toward naphthalene, styrene, and toluene.

Experimental Procedures

Chemicals. Naphthalene, 1-naphthol, 2-naphthol, styrene, styrene 7,8-oxide, toluene, benzylalcohol, *p*-nitrophenol, and 1,2-dihydroxy-4-nitrobenzene were from Wako Pure Chemicals (Osaka, Japan). Chlorzoxazone and 6-hydroxychlorzoxazone were from Sigma-Aldrich (St. Louis, MO). $NADP^+$, glucose-6-phosphate, and glucose-6-phosphate dehydrogenase were purchased from Oriental Yeast (Tokyo, Japan). All other chemicals and solvents were of the highest or analytical grade commercially available.

Enzyme Preparations. *Escherichia coli* (*E. coli*) membranes expressing recombinant human P450/NADPH-P450 reductase (NPR) for P450 1A1 (*24*), 1A2 (*24*), 2A6 (*25*), 2A13 (*26*), and 2E1 (*24*) were prepared as described previously (*25*). The P450 content (*27*) and protein concentration (*28*) were determined according to a method described previously. The NADPH-cytochrome *c* reductase activity was determined as described previously (*29, 30*) using $\Delta_{\varepsilon 550} = 21.1\ mM^{-1}\ cm^{-1}$, and the content was calculated using the specific activity of 3.0 μmol reduced cytochrome *c*/min/nmol NPR based on purified rabbit NPR preparation (*31*). The molar ratios of NPR to P450 were 3.0 (P450 1A1), 0.8 (P450 1A2), 5.8 (P450 2A6), 2.9 (P450 2A13), and 1.3 (P450 2E1), which were sufficiently high to measure the activities as reported previously (*24*).

Enzyme Assays for Naphthalene Hydroxylation and Naphthoquinone Formation from 1-Naphthol. 1- Naphthol and 2-naphthol formation from naphthalene was determined as follows: A typical incubation mixture (0.2 mL total volume) contained an *E. coli* membrane preparation (3 pmol of P450), 100 mM potassium phosphate buffer (pH 7.4), an NADPH-generating system (0.5 mM $NADP^+$, 5 mM glucose-6-phosphate, 5 mM $MgCl_2$, and 1 U/mL glucose-6-phosphate dehydrogenase) and 5–200 μM naphthalene. The reaction was initiated by the addition of the NADPH-generating system after 2-min preincubation at 37 °C. After 5 min of incubation at 37 °C, the reaction was terminated by the addition of 100 μL of cold acetonitrile. After the removal of the protein by centrifugation at 6,500*g* for 5 min, a 20 μL portion of the supernatant was subjected to HPLC. HPLC analyses were performed using an L-7100 pump (Hitachi, Tokyo, Japan), an L-7200 autosampler (Hitachi), and a D-2500 integrator (Hitachi) equipped with a Mightysil RP-18 C18 GP (4.6 × 150 mm; 5 μm) column (Kanto Chemical, Tokyo, Japan). The eluent was monitored at 223 nm with a noise-base clean Uni-3 (Union, Gunma, Japan), which can reduce the noise by integrating the output and increase the signal 3-fold by differentiating the output and 5-fold by further amplification with an internal amplifer, resulting in a maximum 15-fold amplification of the signal. The mobile phase was 30% acetonitrile containing 0.01% phosphoric acid. The flow rate was 1.0 mL/min. The column temperature was 35 °C. The quantification of 1-naphthol and 2-naphthol was performed by comparing the HPLC peak heights with those of authentic standards.

1,2-Naphthoquinone and 1,4-naphthoquinone formation from 1-naphthol was also determined. A typical incubation mixture, reaction condition, and HPLC condition were the same as described above except that 5–200 μM 1-naphthol was added as a substrate, and a 50 μL portion of the supernatant was subjected to HPLC. Once formed, 1,2-naphthoquinone and 1,4-naphthoquinone were effectively reduced by NPR in the membrane of the *E. coli* expression systems. Therefore, instead of the direct estimation with the HPLC peak heights of 1,2-naphthoquinone and 1,4-naphthoquinone, the disappearance of the peak height of the substrate was calculated for the estimation of 1,2-naphthoquinone and 1,4-naphthoquinone formation.

Enzyme Assay for Styrene 7,8-Epoxidation. Styrene 7,8-oxide formation from styrene was determined as follows: a typical incubation mixture (final volume of 0.2 mL) contained an *E. coli* membrane preparation (5 pmol of P450), 100 mM Tris-HCl buffer (pH 7.4), the NADPH-generating system, and 20–1000 μM styrene. The reaction was initiated by the addition of the NADPH-generating system after 2 min of preincubation at 37 °C. After 10 min of incubation at 37 °C, the reaction was terminated by the addition of 10 μL of 60% perchloric acid. After the removal of protein by centrifugation at 9,500*g* for 5 min, a 60 μL portion of the supernatant was subjected to HPLC. The HPLC apparatus was the same as that described above, except for a Capcell Pak C18 UG120 (4.6 × 150 mm, 5 μm) column (Shiseido, Tokyo, Japan). The eluent was monitored at 200 nm with a noise-base clean Uni-3. The mobile phase was 8% acetonitrile containing 0.25% phosphoric acid. The flow rate was 1.0 mL/min. The column temperature was 35 °C. The quantification of styrene 7,8-oxide was performed by comparing the HPLC peak height with that of an authentic standard.

Enzyme Assay for Toluene methyl Hydroxylation. Benzylalcohol formation from toluene was determined as follows: a typical incubation mixture (final volume of 0.2 mL) contained an *E. coli* membrane preparation (5 pmol of P450), 100 mM Tris-HCl buffer (pH 7.4), the NADPH-generating system, and 50–2000 μM toluene. The reaction was initiated by the addition of the NADPH-generating system after 2 min of preincubation at 37 °C. After 5 min of incubation at 37 °C, the reaction was terminated by the addition of 10 μL of 60% perchloric acid. After the removal of protein by centrifugation at 9,500*g* for 5 min, a 60 μL portion of the supernatant was subjected to HPLC. The HPLC apparatus was the same as that described above, except for a Capcell Pak C18 UG120 (4.6 × 250 mm, 5 μm) column. The eluent was monitored at 200 nm with a noise-base clean Uni-3. The mobile phase was 7% acetonitrile containing 0.1% phosphoric acid. The flow rate was 1.0 mL/min. The column temperature was 35 °C. The quantification of benzylalcohol was performed by comparing the HPLC peak height with that of an authentic standard.

Other Enzyme Assays. Chlorzoxazone 6-hydroxylation was determined as described previously (*32*). *p*-Nitrophenol 2-hydroxylation was also determined as described previously (*33*), except that 100 mM potassium phosphate buffer (pH 7.4) was used.

Statistical Analysis. Statistical analyses of the kinetic parameters were performed by two-tailed Student's *t*-test. A value of $P < 0.05$ was considered statistically significant.

Results

Naphthalene Hydroxylation and Naphthoquinone Formation from 1-Naphthol. The catalytic activities of P450 2A13 for 1-naphthol and 2-naphthol formation from naphthalene were measured by comparing them with those of P450 1A1, 1A2, and 2A6. Naphthalene was predominantly converted to 1-naphthol rather than 2-naphthol, in agreement with a previous report (*14*). As shown in Figure 2A and B, P450 2A13 showed the highest activities for these formations. The activities catalyzed by P450 2A6 were similar to those by P450 1A2. P450 1A1 showed the lowest 1-naphthol formation and no 2-naphthol formation. The kinetic parameters of these reactions are summarized in Table 1. For the 1-naphthol formation, the *K*m value of P450 2A13 was similar to those of P450 1A2 and P450 2A6, and the value of P450 1A1 was prominently high. The *V*max value of P450 2A13 was the highest of all four isoforms. Thus, P450 2A13 showed the highest intrinsic clearance. For the 2-naphthol formation, the *K*m value of P450 2A13 was similar

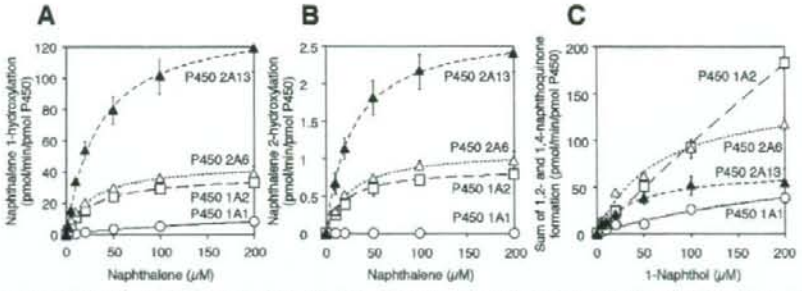

Figure 2. Kinetic analyses of (A) 1-naphthol and (B) 2-naphthol formation from naphthalene, and (*C*) the total formation of 1,2-naphthoquinone and 1,4-naphthoquinone from 1-naphthol catalyzed by recombinant P450 1A1, 1A2, 2A6, and 2A13 expressed in *E. coli*. The kinetic parameters were estimated from the fitted curve using the computer program KaleidaGraph designed for nonlinear regression analysis. Each data point represents the mean of triplicate determinations.

Table 1. Kinetic Parameters for 1-Naphthol and 2-Naphthol Formation from Naphthalene[a]

	*K*m (μM)	kcat (min^{-1})	kcat/*K*m (min^{-1} μM^{-1})
	1-naphthol formation from naphthalene		
P450 1A1	244 ± 45[d]	17 ± 1[d]	0.07 ± 0.01[d]
P450 1A2	29 ± 1	39 ± 1	1.34 ± 0.02
P450 2A6	23 ± 4[c]	43 ± 5	1.90 ± 0.16[d]
P450 2A13	36 ± 2[c]	143 ± 15[d]	4.03 ± 0.58[d]
	2-naphthol formation from naphthalene		
P450 1A1	ND[b]	ND	ND
P450 1A2	19.1 ± 2.5	0.9 ± 0.0	0.05 ± 0.01
P450 2A6	26.5 ± 5.2	1.2 ± 0.1[c]	0.05 ± 0.01
P450 2A13	28.2 ± 2.4[c]	2.9 ± 0.4[d]	0.10 ± 0.00[d]

[a] Data are the mean ± SD of three independent experiments. [b] ND, not detected. [c] $P < 0.05$. [d] $P < 0.005$ compared with P450 1A2.

to that of P450 2A6, but higher than that of P450 1A2. The *V*max value of P450 2A13 was higher than those of P450 1A2 and 2A6. Thus, P450 2A13 showed the highest intrinsic clearance.

The total metabolism of 1-naphthol to 1,2-naphthoquinone plus 1,4-naphthoquinone was determined (Figure 2C), and therefore, the kinetic parameters were not calculated. When the total formation of 1,2-naphthoquinone and 1,4-naphthoquinone by the four P450 isoforms was compared, P450 2A6 showed the highest activity at low substrate concentrations (5–20 μM), but P450 1A2 showed the highest activity at the high substrate concentration (200 μM). At the substrate concentrations of 5–50 μM, P450 2A13 showed activity similar to that of P450 1A2. P450 1A1 showed the lowest activity. Collectively, these results suggested that P450 2A13 has the highest catalytic activity for naphthalene and subsequent 1-naphthol metabolisms.

Styrene 7,8-Epoxidation. The catalytic activity of P450 2A13 for styrene 7,8-oxide formation from styrene was measured by comparing it with those of P450 2E1 and 2A6. As shown in Figure 3A, the activities catalyzed by the three P450s were increased in a substrate concentration-dependent manner. The maximum substrate concentration (1 mM) was not sufficiently high to determine the *K*m values because the solubility of styrene limited the substrate concentration that could be achieved in the incubation mixture. Therefore, the *CL*int values were calculated with the initial slope of the plots of velocity versus substrate concentration. The values in P450 2A13, 2A6, and 2E1 were 46.8, 17.2, and 18.5 min^{-1} mM^{-1}, respectively. These results suggest that P450 2A13 has the highest catalytic activity for styrene 7,8-oxide formation from styrene.

Toluene Methyl Hydroxylation. The catalytic activity of P450 2A13 for benzylalcohol formation from toluene was measured by comparing it with those of P450 2E1 and 2A6. As shown in Figure 3B, the activities catalyzed by the three P450s were increased in a substrate concentration-dependent manner. The maximum substrate concentration (2 mM) was not sufficiently high to determine the *K*m values because the solubility of toluene limited the substrate concentration that could be achieved in the incubation mixture. Thus, accurate kinetic parameters could not be obtained. The *CL*int values calculated with the initial slope of the plots of velocity versus substrate concentration in P450 2A13, 2A6, and 2E1 were 13.3, 2.6, and 5.7 min^{-1} mM^{-1}, respectively. These results suggest that P450 2A13 has the highest catalytic activity for benzylalcohol formation from toluene.

Chlorzoxazone 6-Hydroxylation and *p*-Nitrophenol 2-Hydroxylation. The results of our study prompted us to investigate the possibility that the substrate specificity of P450 2A13 might overlap with that of P450 2E1. The chlorzoxazone 6-hydroxylation and *p*-nitrophenol 2-hydroxylation, which are marker activities of P450 2E1, were measured using recombinant P450 2A13, 2A6, and 2E1. Interestingly, P450 2A13 showed significantly higher catalytic activities for both chlorzoxazone 6-hydroxylation and *p*-nitrophenol 2-hydroxylation than P450 2E1 (Figure 4A and B). As shown in Table 2, the *K*m value for chlorzoxazone 6-hydroxylation by P450 2A13 was approximately one-eighth of that by P450 2E1, and their *V*max values were similar, resulting in 8-fold higher intrinsic clearance than that by P450 2E1. P450 2A6 also catalyzed the chlorzoxazone 6-hydroxylation, but the intrinsic clearance was one-fifth of that by P450 2E1. P450 2A13 catalyzed *p*-nitrophenol 2-hydroxylation with significantly higher (19-fold) intrinsic clearances than that by P450 2E1 (Figure 4B and Table 2) and with a lower *K*m value and higher *V*max value than those of P450 2E1. P450 2A6 also catalyzed the *p*-nitrophenol 2-hydroxylation with clearance similar to that by P450 2E1. These results suggest that P450 2A13 can catalyze the metabolism of P450 2E1 substrates.

Discussion

In the present study, we found that P450 2A13 is catalytically active toward chemicals in air pollutants. P450 2A13 showed significantly higher intrinsic clearances for naphthalene hydroxylation than P450 1A2. Recently, we reported that P450 2A13 is catalytically active toward substrates of P450 1A2, such as aminobiphenyl (*9*), theophylline, and phenacetin (*8*). Especially, it was noteworthy that the catalytic activity of P450 2A13 for phenacetin *O*-de-ethylation was apparently higher than that of P450 1A2. On the basis of the present results, naphthalene

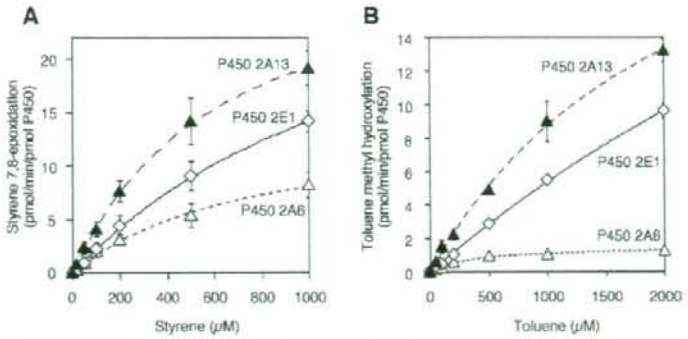

Figure 3. Kinetic analyses of (A) styrene 7,8-oxide formation from styrene and (B) benzylalcohol formation from toluene catalyzed by recombinant P450 2A6, 2A13, and 2E1 expressed in *E. coli*. The styrene and toluene concentrations ranged from 20 to 1000 μM and from 50 to 2000 μM, respectively. Each data point represents the mean of triplicate determinations.

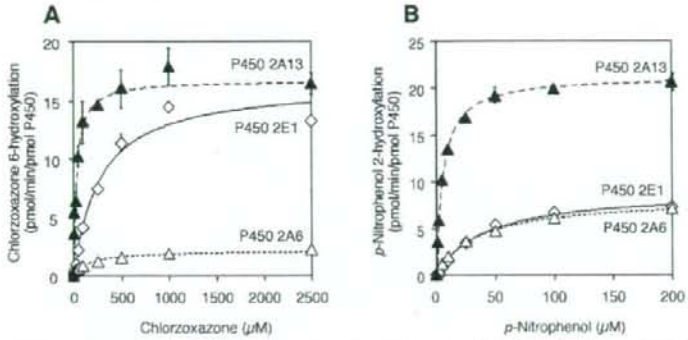

Figure 4. Kinetic analyses of (A) chlorzoxazone 6-hydroxylation and (B) *p*-nitrophenol 2-hydroxylation catalyzed by recombinant P450 2A6, 2A13, and 2E1 expressed in *E. coli*. The kinetic parameters were estimated from the fitted curve using the computer program KaleidaGraph designed for nonlinear regression analysis. Each data point represents the mean of triplicate determinations.

Table 2. Kinetic Parameters for Chlorzoxazone 6-Hydroxylation and *p*-Nitrophenol 2-Hydroxylation[a]

	Km (μM)	kcat (min^{-1})	kcat/Km (min^{-1} μM^{-1})
chlorzoxazone 6-hydroxylation			
P450 2E1	274 ± 18	16.2 ± 0.3	0.06 ± 0.00
P450 2A6	161 ± 19[c]	2.0 ± 0.2[c]	0.01 ± 0.00[c]
P450 2A13	36 ± 4[c]	16.9 ± 1.3	0.47 ± 0.02[c]
p-nitrophenol 2-hydroxylation			
P450 2E1	39.6 ± 0.2	9.1 ± 0.1	0.20 ± 0.00
P450 2A6	30.9 ± 1.9[c]	8.4 ± 0.3[b]	0.27 ± 0.06[b]
P450 2A13	5.5 ± 0.1[c]	20.4 ± 0.6[c]	3.73 ± 0.06[c]

[a] Data are the mean ± SD of three independent experiments. [b] $P <$ 0.05. [c] $P < 0.005$ compared with P450 2E1.

can be added to the P450 2A13 substrates with overlapping substrate specificity with P450 1A2. P450 2A6 also catalyzed naphthalene hydroxylation with similar or higher intrinsic clearance than P450 1A2. A previous study reported that 1-naphthol and 2-naphthol formation from naphthalene in human liver microsomes was inhibited by antibodies toward p450 2a5, mouse orthologue of P450 2A6, to 50–60% and 30–40% of control, respectively (*34*). In addition, Asikainen et al. reported that coumarin 7-hydroxylation in human liver microsomes, a marker activity of P450 2A6, was inhibited by naphthalene in a competitive manner ($K_i = 1.2 - 5.6$ μM) (*34*). Supporting the study, we directly demonstrated that P450 2A6 catalyzes naphthalene hydroxylation.

We found that P450 2A13 showed higher activity for styrene 7,8-oxide formation from styrene than P450 2E1. Styrene 7,8-oxide, which is classified in group 2A (probably carcinogenic to humans) (*18*), is a major reactive metabolite of styrene, and its genotoxicity has been demonstrated by several in vitro test systems (*35, 36*). P450 2A13 also showed higher activity for benzylalcohol formation from toluene, a major detoxification pathway. Toluene is known to be mainly metabolized by P450 2E1. These results suggest that P450 2A13 is active in the metabolism of the P450 2E1 substrates, supported by the fact that P450 2A13 can catalyze chlorzoxazone 6-hydroxylation and *p*-nitrophenol 2-hydroxylation. The bicistronic P450/NPR *E. coli* membranes used in the present study do not include cytochrome b_5. Since it has been reported that the P450 2E1 activity was enhanced by cytochrome b_5 (*24*), we performed a preliminary study to compare the activities of P450 2E1 and 2A13 in the presence of cytochrome b_5. When cytochrome b_5 expressed in *E. coli* was added with equal molar concentration to P450, chlorzoxazone 6-hydroxymation (30 μM substrate concentration) and *p*-nitrophenol 2-hydroxylation (5 μM substrate concentration) catalyzed by P450 2E1 were increased by approximately 2-fold, but these were still considerably (one forth) lower than the activities catalyzed by P450 2A13 in the absence of cytochrome b_5 (Figure S1, Supporting Information). The effects of cytochrome b_5 on styrene 7,8-oxide formation from styrene and benzylalcohol formation from toluene by P450 2E1 and 2A13 were trivial (Figure S1, Supporting Information). Thus, our findings that P450 2A13 showed higher activities toward styrene, toluene, chlorzoxazone, and *p*-nitrophenol were not reversed in the presence of cytochrome b_5. It is generally accepted that P450 2E1 metabolizes a variety of toxins and carcinogens included in air pollutants, such as benzene, xylene,

acrylonitrile, and ethylcarbamate (urethane) (*37*). Therefore, it would be interesting to investigate whether P450 2A13 can catalyze the metabolism of such chemicals in the future.

Recently, Smith et al. (*38*) determined the structure of P450 2A13 by X-ray crystallography and compared it with the structure of P450 2A6. They reported that the overall P450 2A13 and 2A6 structures are very similar. Like 2A6, the P450 2A13 active site is small, planar, and highly hydrophobic with a cluster of phenylalanine residues for $\pi-\pi$ interactions with aromatic ligands. Sansen et al. (*39*) reported that the active site of P450 1A2 is also relatively small and narrow throughout its extent. The X-ray crystallography of P450 2E1 has not yet accomplished, but it is easily assumed that the P450 2E1 active site is relatively small because its substrate molecules are typically small (molecular weight <100). Smith et al. (*38*) reported that the differences in residues 117, 208, 300, and 301 (for definition of the plane of ligands), and residues 365 and/or 366 (for determination of the ligand binding and catalysis) in the active site may be accountable for the difference of substrate specificity between P450 2A13 and 2A6. We cannot compare the residues at comparable sites in P450 1A2 and 2E1 since the overall structures of P450 1A2 and 2E1 are likely to show considerable changes from those of P450 2A6 and 2A13. However, the relative size and planarity of the P450 1A2 active site compared to that of P450 2A13 have some bearing on overlapping substrate specificity.

Naphthalene, styrene and toluene are included in environmental air as hazardous solvents in many industrial workshops and homes. Because they are easily absorbed by inhalation, their local metabolism in the respiratory tract may be as important as that in the liver. P450 2A13 is predominantly expressed in the respiratory tract such as in the lung and trachea (*3, 5*). Recently, the expression of P450 2A13 protein in the epithelia of the bronchus and lung was shown by immunohistochemistry using a P450 2A13-specific antibody (*40*). Therefore, P450 2A13 could play important roles in the metabolic activation or detoxification of numerous procarcinogens and toxicants in air pollutants or tobacco constituents. Since P450 1A1, 2A6, and 2E1 are expressed in the human lung (*41*), they may also contribute to their metabolism. If we can quantitatively compare these expression levels in the human lung, it would be possible to determine which P450 isoform makes the major contribution.

For the *P450 2A13* gene, genetic polymorphisms (http://www.cypalleles.ki.se/cyp2a13.htm) are known. The *P450 2A13*2* allele leading to a substitution of Arg to Cys at the 257 position has been reported to decrease enzyme activities for NNK α-hydroxylation, hexamethylphosphoramide *N*-demethylation, *NN*-dimethylaniline *N*-demethylation, 2′-methoxyacetophenone *O*-demethylation, and *N*-nitrosomethylphenylamine *N*-demethylation (*42*). The *P450 2A13*3* allele causing a frame-shift and *P450 2A13*7* allele having a stop codon at exon 2 (*43*) are predicted to produce the protein lacking enzymatic activity. Wang et al. reported that the *P450 2A13*4* allele leading to a substitution of Arg to Glu at the 101 position caused the lack of protein expression and enzyme activity (*44*). It has been reported that a single nucleotide polymorphism of 7520C > G in the 3′-untranslated region was related to decreased expression in the lung (*45*). The reported association between *P450 2A13* genetic polymorphisms and lung cancer risk is of particular interest (*46, 47*) because P450 2A13 catalyzes the metabolic activation of tobacco-specific carcinogens such as NNK. The genetic polymorphisms of *P450 2A13* might be responsible for the interindividual variability in the carcinogenicity or toxicity of naphthalene, styrene, and toluene.

In conclusion, we found that P450 2A13 can metabolize naphthalene, styrene, and toluene that are included in air pollutants and tobacco smoke. This knowledge increases our understanding of the toxicological significance of P450 2A13 expressed in the respiratory tract.

Acknowledgment. This study was supported in part by a grant from the Smoking Research Foundation in Japan. Tatsuki Fukami was supported as a Research Fellow of the Japan Society for the Promotion of Science. We thank Brent Bell for reviewing the manuscript.

Supporting Information Available: Effects of Cytochrome b_5 on chlorzoxazone 6-hydroxylation, *p*-nitrophenol 2-hydroxylation, styrene 7,8-epoxidation, and toluene methyl hydroxylation catalyzed by P450 2A6, 2A13, and 2E1 (Figure S1). This material is available free of charge via the Internet at http://pubs.acs.org.

References

(1) Fernandez-Salguero, P., Hoffman, S. M. G., Cholerton, S., Mohrenweiser, H., Raunio, H., Rautio, A., Pelkonen, O., Huang, J., Evans, W. E., Idle, J. R., and Gonzalez, F. J. (1995) A genetic polymorphism in coumarin 7-hydroxylation: Sequence of the human *CYP2A* genes and identification of variant *CYP2A6* alleles. *Am. J. Hum. Genet. 57*, 651–660.

(2) Yamano, S., Tatsuno, J., and Gonzalez, F. J. (1990) The CYP2A3 gene product catalyzes coumarin 7-hydroxylation in human liver microsomes. *Biochemistry 29*, 1322–1329.

(3) Su, T., Bao, Z., Zhang, Q. Y., Smith, T. J., Hong, J. Y., and Ding, X. (2000) Human cytochrome P450 CYP2A13: predominant expression in the respiratory tract and its high efficiency metabolic activation of a tobacco-specific carcinogen, 4-(methylnitrosamino)-1-(3-pyridyl)-1-butanone. *Cancer Res. 60*, 5074–5079.

(4) Bao, Z., He, X. Y., Ding, X., Prabhu, S., and Hong, J. Y. (2005) Metabolism of nicotine and cotinine by human cytochrome P450 2A13. *Drug Metab. Dispos. 33*, 258–261.

(5) Koskela, S., Hakkola, J., Hukkanen, J., Pelkonen, O., Sorri, M., Saranen, A., Anttila, S., Fernandez-Salguero, P., Gonzalez, F., and Raunio, H. (1999) Expression of CYP2A genes in human liver and extrahepatic tissues. *Biochem. Pharmacol. 57*, 1407–1413.

(6) Gu, J., Su, Y., Chen, Q. Y., Zhang, X., and Ding, X. (2000) Expression and biotransformation enzymes in human fetal olfactory mucosa: potential roles in developmental toxicity. *Toxicol. Appl. Pharmacol. 165*, 158–162.

(7) He, X. Y., Tang, L., Wang, S. L., Cai, Q. S., Wang, J. S., and Hong, J. Y. (2006) Efficient activation of aflatoxin B_1 by cytochrome P450 2A13, an enzyme predominantly expressed in human respiratory tract. *Int. J. Cancer 118*, 2665–2671.

(8) Fukami, T., Nakajima, M., Sakai, H., Katoh, M., and Yokoi, T. (2007) CYP2A13 metabolizes the substrates of human CYP1A2, phenacetin and theophylline. *Drug Metab. Dispos. 35*, 335–339.

(9) Nakajima, M., Ito, M., Sakai, H., Fukami, T., Katoh, M., Yamazaki, H., Kadlubar, F. F., Imaoka, S., Funae, Y., and Yokoi, T. (2006) CYP2A13 expressed in human bladder metabolically activates 4-aminobiphenyl. *Int. J. Cancer 119*, 2520–2526.

(10) Kulisch, G. P., and Vilker, V. L. (1991) Application of *Pseudomonas pulid* PpG786 containing P-450 cytochrome monooxygenase for removal of trace naphthalene concentrations. *Biotechnol. Prog. 7*, 93–98.

(11) Stucker, I., Bouyer, J., Mandereau, L., and Hemon, D. (1993) Retrospective evaluation of the exposure to polycyclic aromatic hydrocarbons: comparative evaluations with a job exposure matrix and by experts in industrial hygiene. *Int. J. Epidemiol. 22*, 5106–5112.

(12) Vuchetich, P. J., Bagchi, D., Bagchi, M., Hassoun, E. A., Tang, L., and Stohs, S. J. (1996) Naphthalene-induced oxidative stress in rats and the prospective effects of vitamine E succinate. *Free Radical Biol. Med. 21*, 577–590.

(13) Wilson, A. S., Davis, C. D., Williams, D. P., Buckpitt, A. R., Pirmohamed, M., and Park, B. K. (1996) Characterisation of the toxic metabolite. (s) of naphthalene. *Toxicology 114*, 233–242.

(14) Cho, T. M., Rose, R. L., and Hodgson, E. (2006) In vitro metabolism of naphthalene by human liver microsomal cytochrome P450 enzymes. *Drug. Metab. Dispos. 34*, 176–183.

(15) Kanekal, S., Plopper, C., Morin, D., and Buckpitt, A. (1991) Metabolism and cytotoxicity of naphthalene oxide in the isolated perfused mouse lung. *J. Pharmacol. Exp. Ther. 256*, 391–401.

(16) Buckpitt, A., Chang, A. M., Weir, A., Van Winkle, L., Duan, X., Philpot, R., and Plopper, C. (1995) Relationship of cytochrome P450 activity to Clara cell cytotoxicity. IV. Metabolism of naphthalene and naphthalene oxide in microdissected airways from mice, rats and hamsters. *Mol. Pharmacol. 47*, 74–81.

(17) IARC (1989) *Toluene. IARC Monograph on Evaluation of the Carcinogenic Risks of Chemicals to Humans 47*, 79–123, IARC, Vienna, Austria.

(18) IARC (1994) *Styrene. IARC Monograph on Evaluation of the Carcinogenic Risks of Chemicals to Humans 60*, 233–320, IARC, Vienna, Austria.

(19) Bond, J. A. (1989) Review of the toxicology of styrene. *CRC Crit. Rev. Toxicol. 19*, 227–249.

(20) Foo, S. C., Jeyaratnam, J., and Koh, D. (1990) Chronic neurobehavioral effects of toluene. *Br. J. Ind. Med. 47*, 480–484.

(21) Nakajima, T., Elovaara, E., Gonzalez, F. J., Gelboin, H. V., Raunio, H., Pelkonen, O., Vainio, H., and Aoyama, T. (1994) Styrene metabolism by cDNA-expressed human hepatic and pulmonary cytochromes P450. *Chem. Res. Toxicol. 7*, 891–896.

(22) Tassaneeyakul, W., Birkett, D. J., Edwards, J. W., Veronese, M. E., Tassaneeyakul, W., Tukey, R. H., and Miners, J. O. (1996) Human cytochrome P450 isoform specificity in the regioselective metabolism of toluene and *o*-, *m*- and *p*-xylene. *J. Pharmacol. Exp. Ther. 276*, 101–108.

(23) Nakajima, T., Wang, R-S., Elovaara, E., Gonzalez, F. J., Gelboin, H. V., Raunio, H., Pelkonen, O., Vainio, H., and Aoyama, T. (1997) Toluene metabolism by cDNA-expressed human hepatic cytochrome P450. *Biochem. Pharmacol. 53*, 271–277.

(24) Yamazaki, H., Nakamura, M., Komatsu, T., Ohyama, K., Hatanaka, N., Asahi, S., Shimada, N., Guengerich, F. P., Shimada, T., Nakajima, M., and Yokoi, T. (2002) Roles of NADPH-P450 reductase and apo- and holo-cytochrome b_5 on xenobiotic oxidations catalyzed by 12 recombinant human cytochrome P450s expressed in membranes of *Escherichia coli*. *Protein Expression Purif. 24*, 329–337.

(25) Fukami, T., Nakajima, M., Yoshida, R., Tsuchiya, Y., Fujiki, Y., Katoh, M., McLeod, H. L., and Yokoi, T. (2004) A novel polymorphism of human *CYP2A6* gene *CYP2A6*17* has an amino acid substitution (V365M) that decreases enzymatic activity in vitro and in vivo. *Clin. Pharmacol. Ther. 76*, 519–527.

(26) Yamanaka, H., Nakajima, M., Fukami, T., Sakai, H., Nakamura, A., Katoh, M., Takamiya, M., Aoki, Y., and Yokoi, T. (2005) CYP2A6 and CYP2B6 are involved in nornicotine formation from nicotine in humans: interindividual differences in these contributions. *Drug Metab. Dispos. 33*, 1811–1818.

(27) Omura, T., and Sato, R. (1964) The carbon monoxide-binding pigment of liver microsomes. *J. Biol. Chem. 239*, 2370–2378.

(28) Bradford, M. M. (1976) A rapid and sensitive method for the quantitation of microgram quantities of protein utilizing the principle of protein-dye binding. *Anal. Biochem. 72*, 248–254.

(29) Williams, C. H., Jr., and Kamin, H. (1962) Microsomal triphosphopyridine nucleotide-cytochrome c reductase of liver. *J. Biol. Chem. 237*, 587–595.

(30) Yasukochi, Y., and Masters, B. S. (1995) Some properties of detergent-solubilized NADPH-cytochrome c (cytochrome P-450) reductase purified by biospecific affinities chromatography. *J. Biol. Chem. 251*, 5337–5344.

(31) Parikh, A., Gillam, E. M., and Guengerich, F. P. (1997) Drug metabolism by *Escherichia coli* expressing human cytochromes P450. *Nat. Biotechnol. 15*, 784–788.

(32) Court, M. H., Von Moltke, L. L., Shader, R. I., and Greenblatt, D. J. (1997) Biotransformation of chlorzoxazone by hepatic microsomes from humans and ten other mammalian species. *Biopharm. Drug Dispos. 18*, 213–226.

(33) Jiang, Y., Kuo, C. L., Pernecky, S. J., and Piper, W. N. (1998) The detection of cytochrome P450 2E1 and its catalytic activity in rat testis. *Biochem. Biophys. Res. Commun. 246*, 578–583.

(34) Asikainen, A., Tarhanen, J., Poso, A., Pasanen, M., Alhava, E., and Juvonen, R. O. (2003) Predictive value of comparative molecular field analysis modeling of naphthalene inhibition of human CYP2A6 and mouse CYP2A5 enzymes. *Toxicol. in Vitro 17*, 449–455.

(35) Shield, A. J., and Sanderson, B. J. (2004) A recombinant model for assessing the role of GSTM1 in styrene-7,8-oxide toxicity and mutagenecity. *Toxicology 195*, 61–68.

(36) Laffon, B., Perez-cadahia, B., Pasaro, E., and Mendez, J. (2003) Individual sensitivity to DNA damage induced by styrene *in vitro*: influence of cytochrome P450 epoxide hydrolase and glutathione *S*-transferase genotypes. *Toxicology 186*, 131–141.

(37) Guengerich, F. P., Kim, D. H., and Iwasaki, M. (1991) Role of human cytochrome P450 2E1 in the oxidation of many low molecular weight cancer suspects. *Chem. Res. Toxicol. 4*, 168–179.

(38) Smith, B. D., Sanders, J. L., Porubsky, P. R., Lushington, G. H., Stout, C. D., and Scott, E. E. (2007) Structure of the human lung cytochrome P450 2A13. *J. Biol. Chem. 282*, 17306–17313.

(39) Sansen, S., Yano, J. K., Reynald, R. L., Schoch, G. A., Griffin, K. J., Stout, C. D., and Johnson, E. F. (2007) Adaptations for the oxidation of polycyclic aromatic hydrocarbons exhibited by the structure of human P450 1A2. *J. Biol. Chem. 282*, 14348–14355.

(40) Zhu, L. R., Thomas, P. E., Lu, G., Reuhl, K. R., Yang, G. Y., Wang, L. D., Wang, S. L., Yang, C. S., He, X. Y., and Hong, J. Y. (2006) CYP2A13 in human respiratory tissues and lung cancers: an immunohistochemical study with a new peptide-specific antibody. *Drug Metab. Dispos. 34*, 1672–1676.

(41) Shimada, T., Yamazaki, H., Mimura, M., Wakamiya, N., Ueng, Y.-F., Guengerich, F. P., and Inui, Y. (1996) Characterization of microsomal cytochrome P450 enzymes involved in the oxidation of xenobiotic chemicals in human fetal livers and adult lungs. *Drug Metab. Dispos. 24*, 515–522.

(42) Zhang, X., Su, T., Zhang, Q. Y., Gu, J., Caggana, M., Li, H., and Ding, X. (2002) Genetic polymorphisms of the human *CYP2A13* gene: identification of single-nucleotide polymorphisms and functional characterization of an Arg257Cys variant. *J. Pharmacol. Exp. Ther. 302*, 416–423.

(43) Fujieda, M., Yamazaki, H., Kiyotani, K., Muroi, A., Kunitoh, H., Dosaka-Akita, H., Sawamura, Y., and Kamataki, T. (2003) Eighteen novel polymorphisms of the *CYP2A13* gene in Japanese. *Drug Metab. Pharmacokinet. 18*, 86–90.

(44) Wang, S. L., He, X. Y., Shen, J., Wang, J. S., and Hong, J. Y. (2006) The missense genetic polymorphisms of human CYP2A13: functional significance in carcinogen activation and identification of a null allelic variant. *Toxicol. Sci. 94*, 38–45.

(45) Zhang, X., Caggana, M., Cutler, T. L., and Ding, X. (2004) Development of a real-time polymerase chain reaction-based method for the measurement of relative allelic expression and identification of CYP2A13 alleles with decreased expression in human lung. *J. Pharmacol. Exp. Ther. 311*, 373–381.

(46) Wang, H., Tan, W., Hao, B., Miao, X., Zhou, G., He, F., and Lin, D. (2003) Substantial reduction in risk of lung adenocarcinoma associated with genetic polymorphism in CYP2A13, the most activate cytochrome P450 for the metabolic activation of tobacco-specific carcinogen NNK. *Cancer Res. 63*, 8057–8061.

(47) Cauffiez, C., Lo-Guidice, J.-M., Quaranta, S., Allorge, D., Chevalier, D., Cenee, S., Hamdan, R., Lhermitte, M., Lafitte, J.-J., Libersa, C., Colombel, J.-F., Stücker, I., and Broly, F. (2004) Genetic polymorphism of the human cytochrome CYP2A13 in a French population: implication in lung cancer susceptibility. *Biochem. Biophys. Res. Commun. 317*, 662–669.

TX700325F

The Journal of Toxicological Sciences (J. Toxicol. Sci.)
Vol.33, No.4, 405-413, 2008

Original Article

Regulation of insulin-like growth factor binding protein-1 and lipoprotein lipase by the aryl hydrocarbon receptor

Keiichi Minami[1], Miki Nakajima[1], Yuto Fujiki[1], Miki Katoh[1], Frank J. Gonzalez[2] and Tsuyoshi Yokoi[1]

[1]Drug Metabolism and Toxicology, Division of Pharmaceutical Sciences, Graduate School of Medical Science, Kanazawa University, Kanazawa 920-1192, Japan
[2]Laboratory of Metabolism, National Cancer Institute, Bethesda, MD 20892, USA

(Received April 21, 2008; Accepted May 10, 2008)

ABSTRACT — The aryl hydrocarbon receptor (Ahr), a ligand-activated transcriptional factor, mediates the transcriptional activation of a battery of genes encoding drug metabolism enzymes. In the present study, we investigated the hepatic mRNA expression profile in *Ahr*-null (*Ahr* KO) mice compared to wild-type mice by microarray analysis to find new Ahr target genes. Pooled total RNA samples of liver extracted from 7- and 60-week-old *Ahr* KO or wild-type mice were studied by DNA microarray representing 19,867 genes. It was demonstrated that 23 genes were up-regulated and 20 genes were down-regulated over 2 fold in *Ahr* KO mice compared with wild-type mice commonly within the different age groups. We focused on insulin-like growth factor binding protein-1 (Igfbp-1) and lipoprotein lipase (Lpl) that were up-regulated in *Ahr* KO mice. The higher expression in *Ahr* KO mice compared to wild-type mice were confirmed by real-time RT-PCR analysis. In the wild-type mice but not in the *Ahr* KO mice, 2,3,7,8-tetrachlorodibenzo-*p*-dioxin (TCDD) treatment increased the Igfbp-1 and Lpl mRNA levels. The expression profile of Igfbp-1 protein was consistent with that of Igfbp-1 mRNA. Since Lpl is the primary enzyme responsible for hydrolysis of lipids in lipoproteins, the serum triglyceride levels were determined. Indeed, the serum triglyceride levels in *Ahr* KO mice was lower than that in wild-type mice in accordance with the Lpl mRNA levels. Contrary to our expectation, TCDD treatment significantly increased the serum triglyceride levels in wild-type, but did not in *Ahr* KO mice. These results suggest that serum triglyceride levels are not correlated with hepatic Lpl expression levels. In the present study, we found that Ahr paradoxically regulates Igfbp-1 and Lpl expressions in the liver.

Key words: Aryl hydrocarbon receptor, Knockout mice, Igfbp-1, Lpl

INTRODUCTION

Aryl hydrocarbon receptor (Ahr) is a ligand-activated transcription factor and a member of the basic helix-loop-helix/Per-Arnt-Sim (bHLH/PAS) family of chemosensors and developmental regulators. Various kinds of environmental stimuli including 2,3,7,8-tetrachlorodibenzo-*p*-dioxin (TCDD) are well known as ligands of Ahr (Schmidt and Bradfield, 1996; Sogawa and Fujii-Kuriyama, 1997). Upon binding to the ligand, Ahr translocates to the nuclei, coincident with formation of a heterodimeric complex with Ahr nuclear translocator (Arnt). The ligand-activated Ahr mediates the transcriptional activation of a battery of genes encoding enzymes such as cytochrome P450 (CYP) 1 family, NAD(P)H: quinone oxidoreductase and glutathione *S*-transferase Ya subunit that function in the metabolism of xenobiotics and endobiotics (Bock, 1994; Rowlands and Gustafsson, 1997).

Gene knockout technology is a useful tool to estimate the roles of certain genes *in vivo*. *Ahr*-null (*Ahr* KO) mice on a C57BL/6 strain background were established by three research groups (Fernandez-Salguero *et al.*, 1995; Schmidt *et al.*, 1996; Mimura *et al.*, 1997). The *Ahr* KO mice established by Fernandez-Salguero *et al.* (1995) exhibited 40-50% neonatal lethality, although survivors reached maturity and were fertile. The *Ahr* KO mice established by the latter two groups exhibited no neonatal lethality, but the growth rate was decreased in the first few weeks. In the *Ahr* KO mice, the size of the liver has been reported to be decreased compared with

Correspondence: Tsuyoshi Yokoi (E-mail: tyokoi@kenroku.kanazawa-u.ac.jp)

that in wild-type mice (Fernandez-Salguero *et al.*, 1995; Schmidt *et al.*, 1996). Hepatic portal fibrosis and hepatic vascular hypertrophy were observed in the *Ahr* KO mice (Fernandez-Salguero *et al.*, 1995; Fernandez-Salguero *et al.*, 1997). In addition, the accumulation of retinoid in the liver owing to reduced retinoic acid metabolism has also been documented (Andreola *et al.*, 1997). The abnormality of retinoid homeostasis was considered to be the reason for the liver fibrosis in the *Ahr* KO mice (Andreola *et al.*, 2004). Zaher *et al.* (1998) found that transforming growth factor β is overexpressed in the liver of *Ahr* KO mice, and this could be a causal factor of liver fibrosis. Thus, these findings suggest that Ahr expression in the liver is important for normal liver development. In the present study, we sought to determine the hepatic mRNA expression profile in *Ahr* KO mice compared with that in wild-type mice by microarray analysis to identify new targets of Ahr.

MATERIALS AND METHODS

Chemicals

CodeLink™ Expression Assay Reagent kit, Manual Prep and streptavidin-Cy5 were purchased from GE Healthcare Bio-Sciences (Piscataway, NJ, USA). QIAquick PCR Purification Kit and RNeasy Mini Kit were from Qiagen (Hilden, Germany). NEN Blocking Reagent and Biotin 11-UTP were from Perkin-Elmer Life Sciences (Boston, MA, USA). ReverTra Ace (Moloney Murine Leukemia Virus Reverse Transcriptase RNase H Minus) was from Toyobo (Osaka, Japan). SYBR Premix Ex Taq (Perfect Real Time) was from Takara (Shiga, Japan). Goat anti-mouse insulin-like growth factor binding protein 1 (Igfbp-1) antibody was purchased from Santa Cruz Biotechnology (Santa Cruz, CA, USA). Triglyceride E Test Wako was from Wako Pure Chemical Industries (Osaka, Japan). TCDD was from Cambridge Isotope Laboratories (Cambridge, MA, USA). All primers were commercially synthesized at Hokkaido System Sciences (Sapporo, Japan). Other chemicals were of the highest grade commercially available.

Animals and treatment

Ahr KO mice generated by Fernandez-Salguero *et al.* (1995) were used. Animals were housed in the institutional animal facility in a controlled environment (temperature 25 ± 1°C, humidity 50 ± 10% and 12 hr light/12 hr dark cycle) with access to food and water *ad libitum*. Animal maintenance and treatment were conducted in accordance with the National Institutes of Health Guide for Animal Welfare of Japan, as approved by the Institutional Animal Care and Use Committee of Kanazawa University. Genotyping of animals was carried out by polymerase chain reactions (PCRs) described previously (Takemoto *et al.*, 2004). For the DNA microarray experiment, 7- and 60-week-old *Ahr* KO and wild-type mice were used. For the TCDD treatments, TCDD in corn oil (40 μg/kg body weight per day) was intraperitoneally administered to 35-week-old *Ahr* KO mice and 14-week-old wild-type mice for four days. Corn oil (2 ml/kg body weight) was administered as a control.

Total RNA preparation

Mice were sacrificed and the livers were collected and immediately frozen in liquid nitrogen and stored at −80°C until use. Total RNA from liver was isolated using ISOGEN (Nippon Gene, Tokyo, Japan) according to the manufacturer's protocol. Equal amounts of total RNA from 5 - 7 mice were pooled.

Microarray analysis

Microarray analysis was performed using a CodeLink™ Bioarray Perfect System according to the manufacturer's protocol (GE Healthcare Bio-Sciences). A Codelink™ UniSet Mouse 20K I Bioarray (GE Healthcare Bio-Sciences) consisting of 19,867 genes including expression sequence tags (ESTs) was used. Processed slides were scanned with an Agilent G2565BA Microarray Scanner using Agilent Scan Control Software (Agilent Technologies, Palo Alto, CA, USA) with the laser set to red (633 nm) and the photomultiplier tube value to 70%. The scanned images for each slide were analyzed using CodeLink™ Expression Analysis Software (GE Healthcare Bio-Sciences). The microarray data quality control was as follows: present, no flags (neither marginal nor absent); marginal, low quality spots judged by analysis software; absent, low signal density spots. Microarray data management was performed with GeneSpring software (Agilent Technologies). Comparison of the present genes, expression filtering and experiment normalization were performed. The individual gene expression for each array was normalized to their respective median value. Expression filters included the requirement that the genes be present in over 200% of controls for up-regulated genes and below 50% of controls for down-regulated genes.

Real-time RT-PCR

Total RNA (4 μg) was reverse transcribed using ReverTra Ace according to the manufacturer's instructions and the resulting cDNA was amplified by PCR. Real-time PCR was performed using the Smart Cycler (Cepheid,

Sunnyvale, CA, USA). PCR reactions were carried out as follows: A 1 μl portion of the reverse transcribed mixture was added to a PCR mixture containing 0.4 μM of each primer and SYBR Premix Ex Taq solution in a final volume of 25 μl. The primers used for PCR are shown in Table 1. The PCR condition for *Igfbp-1*, *Lpl*, *Cyp17a1*, and *GAPDH* was as follows: after an initial denaturation at 95°C for 30 sec, the amplification was performed by denaturation at 94°C for 4 sec, annealing and extension at 64°C for 20 sec for 45 cycles. The amplified products were monitored directly by measuring the increase of the dye intensity of the SYBR Green I. To normalize RNA loading and PCR variations, the signals of targets were corrected with the signals of GAPDH mRNA as the internal standard.

Western blot analysis of Igfbp-1

Ahr KO and wild-type mice were sacrificed 24 hr after the last treatment with TCDD. The livers were homogenized with buffer (0.1 M Tris-HCl (pH 7.4), 0.1 M KCl, 1 mM EDTA, 1 mM Na_3VO_4, 1 mM NaF) and liver homogenates (100 μg protein) subjected to SDS-polyacrylamide gel electrophoresis with 10% polyacrylamide gels followed by Western blotting using a PVDF membrane (Immobilon-P, Millipore, Billerica, MA, USA). The membrane was incubated with goat anti-Igfbp-1 antibody at a dilution of 1:200. Biotinylated anti-goat IgG and a VECTASTAIN ABC kit (Vector Laboratories, Burlingame, CA) were used for diaminobenzidine staining. The quantitative analysis of protein expression was performed using ImageQuant TL software (GE Healthcare Bio-Sciences).

Serum triglycerides concentration

Blood samples were collected from the postcaval vein 24 hr after the last treatment with TCDD. The serum triglyceride concentration was measured using Triglyceride E Test Wako.

Table 1. Primers used in the present study.

Primer	Sequence
Cyp17a1 S	5'-GTA TTC AGC ACC TTT TCC CT-3'
Cyp17a1 AS	5'-AAT ATG TCC ACC AGA TCG CT-3'
IGFBP-1 S	5'-CAA ACT GCA ACA AGA ATG G-3'
IGFBP-1 AS	5'-TGT ATC AAG CAG TAT GTG G-3'
LPL S	5'-AGA AGC AGC AAG ATG TAC CT-3'
LPL AS	5'-GAA ACT TTC TCC CTA GCA CA-3'
GAPDH S	5'-AAA TGG GGT GAG GCC GGT-3'
GAPDH AS	5'-ATT GCT GAC AAT CTT GAG TGA-3'

Statistical analysis

Statistical significance was determined by analysis of variance (ANOVA) followed by Dunnett's test for multiple comparisons.

RESULTS

Comparison of gene expression profiles in Ahr KO and wild-type mice

Among 19,867 genes, 11,509 (58%) genes were categorized into 15 groups (Table 2). Among these, 7,255 (37%) genes showed sufficient spot density. In 7-week-old *Ahr* KO mice, the expression levels of 133 genes were elevated, whereas those of 95 genes were suppressed compared with age-matched wild-type mice. In 60-week-old *Ahr* KO mice, the expression levels of 76 genes were elevated, whereas those of 136 genes were suppressed compared with age-matched wild-type mice. In both 7- and 60-week-old *Ahr* KO mice, 23 genes were commonly elevated and 20 genes were commonly suppressed. The 43 common genes are shown in Table 3. Cyp1a2 and Ugt1a6, which are known to be highly regulated by Ahr, were down-regulated in *Ahr* KO mice. In addition, we found that Slc22a7 (organic anion transporter 2, Oat2) and Slc2a2 (facilitated glucose transporter 2) were also down-regulated in *Ahr* KO mice. These results suggest that these genes might be targets of Ahr regulation.

The expression levels of methylmalonyl-Coenzyme A mutase, lipoprotein lipase (Lpl), and Cyp17a1 were highly (over 10 fold in 7-week-old mice) up-regulated in *Ahr* KO mice. Among these, the spot density of Lpl was highest. We additionally found that Igfbp-1 was unexpectedly up-regulated in *Ahr* KO mice, because previous studies reported that *Igfbp-1* mRNA was induced by TCDD via Ahr activation (Adachi *et al.*, 2004, Marchand *et al.*, 2005). In a subsequent study, we investigated in detail the expression of Igfbp-1 and Lpl in the liver.

Real-time RT-PCR analysis

To confirm the results of the DNA microarray analysis, real-time RT-PCR analysis was performed (Fig. 1). The hepatic *Igfbp-1* mRNA levels in *Ahr* KO mice were 7 fold (7-week-old) and 24 fold (60-week-old) higher than those in age-matched wild-type mice. The hepatic *Lpl* mRNA levels in *Ahr* KO mice were 8 fold (7-week-old) and 3 fold (60-week-old) higher than those in age-matched wild-type mice. Thus, the differences in the expression levels detected by microarray analysis were reproducible.

Table 2. Number of genes of which expression were significantly changed in *Ahr* KO mice.

Category	Total [1]	Present [2]	Up-regulated (> 2 fold)			Down-regulated (< 2 fold)		
			7 w	60 w	7 & 60 w	7 w	60 w	7 & 60 w
Apoptosis regulator	265	198	5	3	0	0	5	0
Cancer	168	109	2	2	2	1	2	0
Cell cycle	386	252	5	3	1	0	0	0
Chaperone	429	276	4	3	0	4	9	0
Enzyme	3,829	2,615	59	28	12	54	59	11
Immunity	143	93	1	1	0	2	2	1
Microtubular	63	38	0	0	0	0	0	0
Motor	40	24	2	1	1	0	0	0
Nucleic acid binding	1,812	1,183	18	6	0	9	17	0
RNA	14	12	0	0	0	0	0	0
Signal transducer	839	387	6	6	2	7	6	1
Storage	11	5	0	0	0	0	0	0
Structural protein	1,341	700	17	11	3	7	11	2
Transport	1,465	955	11	9	2	10	20	5
Others	704	408	3	3	1	1	5	0
	11,509	7,255	133	76	23	95	136	20

Up-regulated and down-regulated genes showed more than 200% expression and less than 50% expression, respectively, compared with those in wild type mice.

[1] Number of genes of which categories were defined.

[2] Number of genes showing enough spot density.

Effects of TCDD treatment on Igfbp-1 and Lpl mRNA expression in *Ahr* KO and wild-type mouse livers

We investigated the effect of TCDD treatment on *Igfbp-1* and *Lpl* mRNA expressions. Real-time RT-PCR analyses revealed that *Igfbp-1* mRNA was significantly (7 fold) increased by TCDD in wild-type mice, but not in *Ahr* KO mice, showing 8-fold higher *Igfbp-1* mRNA levels than those in wild-type mice (Fig. 2A). *Lpl* mRNA was also significantly (4 fold) increased by TCDD in wild-type mice, but not in *Ahr* KO mice, showing 4-fold higher *Lpl* mRNA levels than those in wild-type mice (Fig. 2B).

Igfbp-1 protein expression

Western blot analysis demonstrated that Igfbp-1 protein was significantly (5 fold) induced by TCDD in wild-type mice (Fig. 3), but not in *Ahr* KO mice, showing 6-fold higher Igfbp-1 protein levels.

Triglycerides concentration measurement

Since an antibody against Lpl is not commercially available, we sought to determine the Lpl activity to evaluate changes in the hepatic Lpl expression level. Lpl is the primary enzyme responsible for the metabolism of triglycerides. We investigated whether the differences in the Lpl expression level in liver might be inversely correlated with the serum triglyceride levels. The serum triglyceride level was lower in *Ahr* KO mice than in wild-type mice, being inversely correlated with the Lpl expression level. However, the serum triglyceride level was significantly (1.3 fold) increased by TCDD treatment in wild-type mice, but not in *Ahr* KO mice (Fig. 4).

DISCUSSION

DNA microarray technology has been extensively used as a powerful tool for predicting unknown signaling pathways. Using DNA microarray analysis, the changes in mRNA expression levels in smooth muscle cells in *Ahr* KO mice were investigated by Guo *et al.* (2004) who found that transforming growth factor-beta 3 (*Tgfb3*) expression was higher in *Ahr* KO mice than in wild-type mice, indicating that Ahr suppresses *Tgfb3* gene expression. It is well known that Ahr regulates various drug-

Table 3. Up- or down-regulated genes in *Ahr* KO mice.

Gene name	Genbank ID	Common name	Relative mRNA expression 7 w	60 w
Up regulation (23 genes)				
Cancer				
Rab38, member of RAS oncogene family	NM_028238	Rab38	2.1	4.3
Vav2 oncogene	NM_009500	Vav2	2.1	2.2
Cell cycle regulator				
Cyclin B2	NM_007630	Ccnb2	3.8	2.1
Enzyme				
Aldo-keto reductase family 1, member B7	NM_009731	Akr1b7	2.0	2.6
Arylacetamide deacetylase (esterase)	NM_023383	Aadac	2.5	2.0
Asparagine synthetase	U38940	Asns	6.5	5.0
Cis-retinol/3alpha hydroxysterol short-chain dehydrogenase-like	BC018263	CRAD-L	3.2	3.1
Cytochrome c oxidase, subunit VIIa 1	NM_009944	Cox7a1	2.8	2.1
Cytochrome P450, family 4, subfamily a, polypeptide 14	NM_007822	Cyp4a14	3.6	4.1
Cytochrome P450, family 17, subfamily a, polypeptide 1	NM_007809	Cyp17a1	12.5	2.1
Glutaredoxin 2 (thioltransferase)	NM_023505	Glrx2	2.3	2.2
Hydroxysteroid (17-beta) dehydrogenase 9	NM_013786	Hsd17b9	3.0	3.5
Lipoprotein lipase	NM_008509	Lpl	14.0	5.5
Methylmalonyl-Coenzyme A mutase	NM_008650	Mut	23.6	9.8
RIKEN cDNA 2310016A09 gene	BC024580	RIKEN	4.7	2.7
Motor				
Dynein, axonemal, intermediate chain 1	AK004387	Dnaic1	4.1	8.2
Signal transducer				
Insulin-like growth factor binding protein 1	NM_008341	Igfbp1	3.2	4.8
Structural protein				
CD59a antigen	NM_007652	Cd59a	8.4	3.7
Collectin sub-family member 11	AK003121	Colec11	2.2	2.3
Olfactory receptor 65 (Olfr65)	NM_013617	Olfr65	2.3	2.5
Transport				
Fatty acid binding protein 5, epidermal	NM_010634	Fabp5	2.3	2.7
Solute carrier organic anion transporter family, member 1a4	NM_030687	Slco1a4	2.9	2.3
Others				
Ubiquitin-associated protein 1	NM_023305	Ubap1	5.8	3.3

Table 3. (Continued)

Gene name	Genbank ID	Common name	Relative mRNA expression 7 w	60 w
Down regulation (20 genes)				
Enzyme				
Betaine-homocysteine methyltransferase	NM_016668	Bhmt	0.48	0.49
Cytochrome P450, family 1, subfamily a, polypeptide 2	NM_009993	Cyp1a2	0.30	0.36
Dopachrome tautomerase	NM_010024	Dct	0.26	0.32
Glutathione peroxidase 6	NM_145451	Gpx6	0.45	0.37
Interferon gamma-induced GTPase	NM_018738	Igtp	0.28	0.27
Isovaleryl coenzyme A dehydrogenase	NM_019826	Ivd	0.16	0.18
NADH dehydrogenase (ubiquinone) Fe-S protein 5	NM_134104	Ndufs5	0.02	0.01
Sulfotransferase family 5A, member 1	NM_020564	Sult5a1	0.30	0.29
UDP glucuronosyltransferase 1 family, polypeptide A6	U16818	Ugt1a6	0.38	0.48
Expressed sequence AI586015	NM_019992	AI586015	0.26	0.42
RIKEN cDNA E430034L04 gene	NM_011816	RIKEN	0.43	0.42
Immunity				
Plasminogen	NM_008877	Plg	0.49	0.40
Signal transducer				
Transforming growth factor beta 1 induced transcript 4	NM_009366	Tgfb1i4	0.23	0.46
Structural protein				
Growth arrest specific 5	NM_013525	Gas5	0.27	0.46
Prion protein	NM_011170	Prnp	0.48	0.50
Transport				
Amiloride-sensitive cation channel 5, intestinal	NM_021370	Accn5	0.12	0.23
Aquaporin 8	NM_007474	Aqp8	0.46	0.39
Solute carrier family 2 (facilitated glucose transporter), member 2	NM_031197	Slc2a2	0.47	0.26
Solute carrier family 22 (organic anion transporter), member 7	NM_144856	Slc22a7	0.35	0.47
Sorting nexin 1	NM_019727	Snx1	0.42	0.45

Up-regulated and down-regulated genes showed more than 200% and less than 50% expressions, respectively, compared with those in wild-type mice at the same weeks old.

Categories of first occurrence in Table 2 are listed.

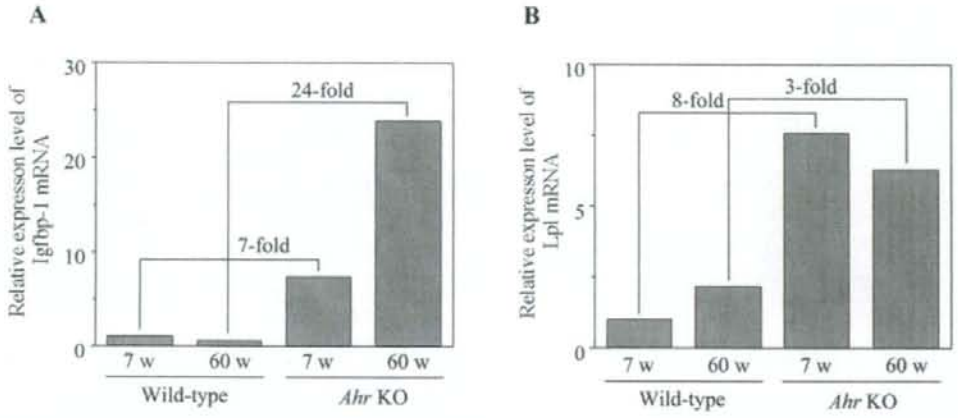

Fig. 1. Relative expression levels of (A) *Igfbp-1* and (B) *Lpl* mRNA in the liver of *Ahr* KO and wild-type mice determined by real-time RT-PCR. Total RNA was extracted from 7- and 60-week-old *Ahr* KO or wild-type mice. Samples from 5 - 7 mice were pooled within each group. The expression levels of *Igfbp-1* and *Lpl* mRNA were normalized with the expression level of GAPDH as a control. Data are expressed as the mean of duplicate experiments.

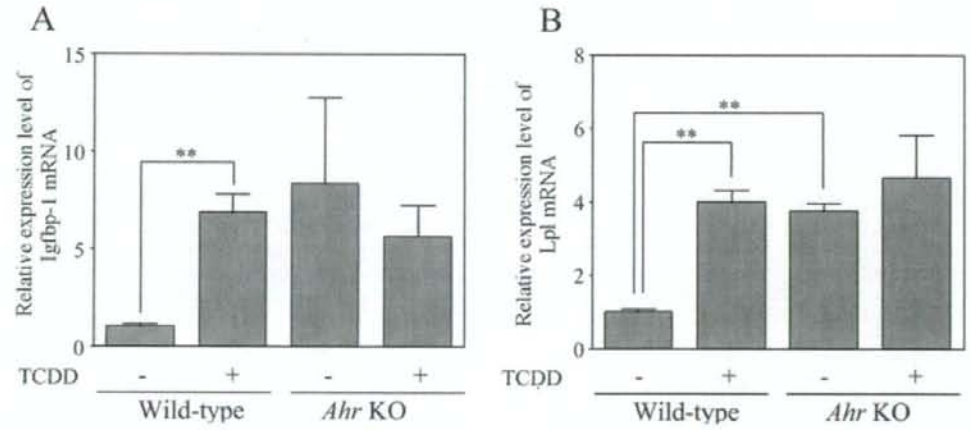

Fig. 2. Effects of TCDD treatment on the expression levels of (A) *Igfbp-1* and (B) *Lpl* mRNA in the liver of *Ahr* KO and wild-type mice determined by real-time RT-PCR analysis. TCDD (40 μg/kg weight) or corn oil was intraperitoneally administered to *Ahr* KO (35-week-old) and wild-type (14-week-old) mice for 4 days. The expression levels of *Igfbp-1* and *Lpl* mRNA were normalized with the expression level of GAPDH as a control. Data are expressed as mean ± S.E. from 5 or 6 mice. $^{**}P < 0.01$ by ANOVA.

metabolizing enzymes in liver. In the present study, we sought to investigate the mRNA profiles in liver from *Ahr* KO mice using microarray to find new Ahr gene targets. The overall gene expression profiles vary during development and the aging process. Therefore, we compared the data in young (7-week-old) and older (60-week-old) mice to determine common changes in gene expression by *Ahr* KO. The decreases in Cyp1a2 and Ugt1a6 in *Ahr* KO mice were consistent with those previously reported (Fernandez-Salguero *et al.*, 1995). In addition, the

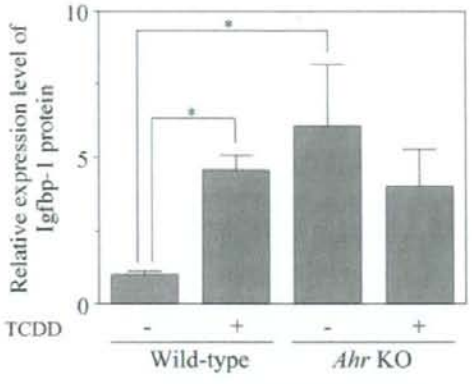

Fig. 3. Effects of TCDD treatment on the expression level of Igfbp-1 protein level in the liver of *Ahr* KO and wild-type mice. TCDD (40 μg/kg weight) or corn oil was intraperitoneally administered to *Ahr* KO (35-week-old) and wild-type (14-week-old) mice for 4 days. Data are expressed as mean ± S.E. from 5 or 6 mice. $^{*}P < 0.05$ by ANOVA.

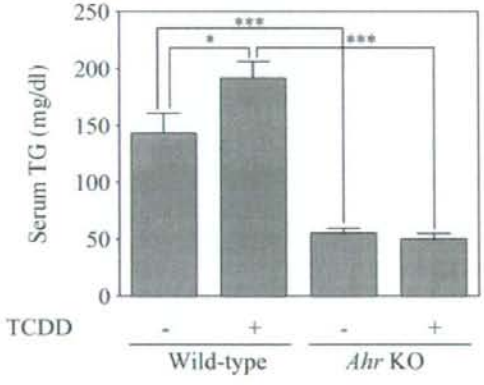

Fig. 4. Effects of TCDD treatment on serum triglyceride level in *Ahr* KO and wild-type mice. TCDD (40 μg/kg weight) or corn oil was administered to *Ahr* KO (35-week-old) and wild-type (14-week-old) mice for 4 days. Data are expressed as mean ± S.E. from 5 or 6 mice. $^{*}P < 0.05$, $^{***}P < 0.001$ by ANOVA.

decrease of Slc22a7 and increase of Cyp17a1 in livers in *Ahr* KO mice were consistent with a recent report by Tijet *et al.* (2006). These results suggest that our study was sufficiently reliable. In the present study, we first found that the *Igfbp-1* and *Lpl* expression levels were higher in *Ahr* KO mice.

Despite the fact that the expression levels of Igfbp-1 and Lpl in the liver were increased in the *Ahr* KO, they were induced by TCDD in an Ahr-dependent manner. The latter results suggested that Ahr positively regulates Igfbp-1 and Lpl in the presence of the ligands. This is supported by a previous report indicating that a xenobiotic responsive element (XRE) to which Ahr binds is located in the promoter region of the *Igfbp-1* gene at -87 (Marchand *et al.*, 2005). In addition, we found two XRE sequences in the promoter region of the *Lpl* gene at -332 and -443 by a computer-assisted homology search. Further study will be necessary to determine whether the binding of Ahr to XRE might be responsible for the induction of Lpl by TCDD. Based on the higher expression levels of Igfbp-1 and Lpl in *Ahr* KO mice compared to those in the wild-type mice, Ahr might suppress Igfbp-1 and Lpl expressions in the absence of exogenous ligands and TCDD may interfere with the suppression. Alternatively, Ahr might positively regulate some suppressor of Igfbp-1 and Lpl expression in the absence of exogenous ligands.

IGFBP-1, one of the six IGFBPs, capable of sequestering insulin growth factors (IGF)s from their receptor. It was reported that transgenic mice of human *IGFBP-1* gene showed postnatal growth retardation and impaired fecundity (Schneider *et al.*, 2000). The pathophysiological abnormalities in *Ahr* KO mice such as decreased body weight, impaired fecundity as well as decrease liver size (Fernandez-Salguero *et al.*, 1995) might be, in part, associated with Igfbp-1 overexpression.

LPL is produced by adipose tissue and then is transported to the endothelial cell surface (Matsumura, 1995). It is also expressed in heart, lung, adipose tissue, kidney, intestine and liver in mice (Kirchgessner *et al.*, 1987). Lpl hydrolyses triglycerides. In *Ahr* KO mice, Lpl expression in adipocytes might also be increased in addition to that in liver, because the serum triglyceride levels in *Ahr* KO mice were decreased. The serum triglyceride level was increased by TCDD treatment in wild-type mice, being consistent with a previous report showing that adipose Lpl activity was decreased by TCDD treatment (Matsumura, 1995). TCDD inhibits the differentiation of preadipocytes to adipocytes (Alexander *et al.*, 1998). The differentiation increases peroxisome proliferator activated receptor (PPAR) γ expression, which is a major regulator of Lpl in adipocytes. Therefore, the increase of serum triglycerides by TCDD in wild-type mice was, in part, due to the inhibition of adipogenesis.

In summary, we found that hepatic Igfbp-1 and Lpl were paradoxically up-regulated by the activation and